Comparative Study of the Material Point Method and Smoothed Particle Hydrodynamics Applied to the Numerical Simulation of a Dam-Break Flow in the Presence of Geometric Obstacles

Manuel Vargas[1], Elson Nascimento[1], Gabriel Nascimento[1*], Marcelo Hotta[2]
and Marcio Almeida[2]

[1]*Federal Fluminense University, Rua Passos da Patria 156, Niterói/RJ – 24210330, Brazil.*
[2]*Federal University of Rio de Janeiro, Av. Pedro Calmon, 550, Rio de Janeiro/RJ – 21941901, Brazil.*

Authors' contributions

This work was carried out in collaboration between all authors. Author MA designed the study and managed the revision with Author MH. Authors EN and GN supervised the work and performed the first numerical analysis. Author MV continued the study with further numerical analysis and wrote the first draft of the manuscript. All authors read and approved the final manuscript.

Original Research Article

ABSTRACT

Dam break is one of the greatest hazards causing damages in urban and rural areas throughout the world. It can happen due to design and construction errors, heavy rainfall, earthquakes or glacier melting, among other reasons. Once the dam collapses, the resulting flow can become even worse due to obstacles, like houses, walls, bridges and trees, which can be impacted and transported along with the water. The prevention or reduction of the downstream effects of a dam break due to the complex and highly energized flow has been a challenge to researchers and engineers all over the world. The present study aimed to compare two free computer programs for numerical simulation of a flow with obstacles, based on available experimental data. These programs are

_____

*Corresponding author: E-mail: gabrielcn@id.uff.br;

based on the material point method (MPM) and smoothed particle hydrodynamics (SPH), respectively. The numerical results of the two programs were in good agreement with experimental data, although important differences in computing time were observed. Therefore, these methods seem to be potential tools for the prediction of dam-break flows.

1. INTRODUCTION

Since its formation, the Earth has constantly been threatened by natural hazards such as earthquakes, tsunamis, floods, storms, volcanic eruptions and landslides. When these hazards turn into catastrophic natural disasters, they can cause loss of life, major environmental damage, and even total destruction of everything in their path [1]. The most prevalent natural hazards are earthquakes, storms and floods. The first is caused by movements of the tectonic plates, while the last two are due to climatic effects [1,2].

Earthquakes can also cause dam breaks and consequent flooding. Considering that 43% of the natural disasters are due to flooding (Fig. 1), created by high rainfall, or in some places of the world by the glacier melting, these are among the most significant concerns of civil engineers involved in their design and construction. The most common cause of a dam break is exceeding the water volume limit related to the structural resistance of the dam and related inappropriate human interventions.

Throughout history, there have been many cases of dam breaks [3]. The most destructive to date was in 1975 in Henan Province, China, when the Banquiao Dam and the Shimantan Dam failed catastrophically due to overtopping caused by torrential rains. As a consequence, approximately 85,600 people died and millions of residents lost their homes [4,5]. Experts announced that the floodgates opened, but these were partially blocked by the accumulated sediments, which prevented the release of water and led the dams to collapse [5].

For this reason, the prevention of dam breaks has been a relevant theme of research for many decades, due to the high levels of human and material losses caused by the resulting floods [1]. The degree of flood damage may be greater or smaller depending on the topography, downstream obstacles, the way of fluid propagates and the success of evacuation efforts. The obstacle factor is directly related to the presence of houses, walls, bridges and trees, among others. This is an important point to consider, due to variations in velocities, force, depth, direction and behavior of the fluid at the moment of impacting the obstacle, transforming this impact energy into shock waves of different heights and danger levels.
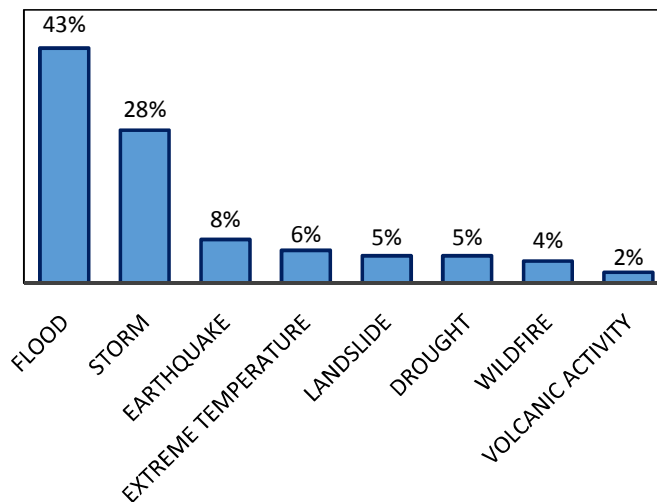
Fig. 1. Percentage of occurrences of natural disasters [1995-2015], adapted from R. Davies [2]

2. BACKGROUND AND OBJECTIVES

The transport of sediments and erosion producing dam breaks has been a topic of research by many authors (e.g., see [6–36]). For example, Singh et al. [6] studied the evolution of dam breach and the subsequent flood and sediment routing. The same authors a year later [7] analyzed dam-breach erosion for rectangular and triangular breach sections and tested it using two historical cases. Martin N.R et al. [9] analyzed the effect of check dams according to different concepts on debris flow dynamics or debris flow prevention. David et al. [12] characterized the quantity of sediment mobilized and transported by dam-break flow. Zhixian et al. [17] presented a numerical model for dam-break flow, sediment transport, and morphological evolution. In 2007, Faeh et al. [18] presented a numerical model of breach erosion of river embankments to show the impact of different processes and input parameters on the breach outflow of a granular embankment failure.

Shakibaeinia et al. [24] proposed a new non-Newtonian multiphase model (involving properties of the sediment phase) based on the WC-MPS formulation to model the mobile dam-break problem. Li et al. [27] presented a physically enhanced layer-averaged model for dam-break flow, sediment transport and morphological evolution. In 2015, Evangelista et al. [34] presented some laboratory experimental results of erosion of a sand dike produced by the impact of a dam-break wave. Fu et al. in 2016 [35] studied numerical models of sediment transport under dam flow conditions using the multiphase particle method and Di Cristo et al. in 2017 [36] analyzed the idealized case of a wave frontally hitting a loose sediment embankment both experimentally and numerically.

The work presented in this article is based on an idealization of the dam break problem, which does not consider sediment transport, also called fixed bed condition. In the bibliographic review for a dam break with fixed bed, we found several articles by different researchers (e.g., see [37–98]), which through experimental studies and numerical simulations have analyzed and explained with great precision the behavior, depth and time of arrival of the fluid.

In the mentioned literature, Dressler et al. [38] investigated the hydraulic resistance effect on the dam-break functions. In 1954, the same research group [39] compared theories and experiments for hydraulic dam-break waves. Xanthopoulos et al. [40] studied, with the aid of a numerically solved mathematical model, the inundation of a real, nearly flat plain, by a flood hydrograph created by a dam failure and loading of the plain from a peripheral point. Katopodes [41] presented and compared five dam-break flood wave models, which were all either originally developed or reconstructed by the authors in order to assure inter-model consistency. Townson et al. [42] applied the feature method in a radial flow condition for a dam break, especially for parallel, convergent and divergent combinations of boundaries, both upstream and downstream. Soulis [44] improved their own research on steady two-dimensional subcritical-supercritical flow for open channel calculations. Fraccarollo et al. [45] reported a numerical and experimental investigation of a three-dimensional dam-break model.

Adopting the two-dimensional shallow water equations as the mathematical description of the problem and applying the weighted averaged flux method, Wang et al. [48] assessed and demonstrated the applicability of a Lagrangian discrete parcel method to discontinuous 1 D open channel flow. Colicchio et al. [49] presented a comparative study between the boundary-element method for potential flow, the smoothed particle hydrodynamics method for Euler equations and the direct solution of the Navier-Stokes equations coupled with the level set method to capture the free surface. In 2005, Quecedo et al. [53] compared two mathematical models, the first to solve the Navier-Stokes equations and the second to solve shallow water equations.

To solve the dam-break problem using the finite element method, Cruchaga et al. [58] presented numerical and experimental analyses of the collapse of a liquid column. The experiments were performed by two types of fluids: shampoo and water. Soarez et al. analyzed the ability of a finite-volume numerical model, commonly used in inundation modeling, to reproduce fast transient flows including multiple interactions with obstacles. Ozmen-Cagatay [70] acquired accurate laboratory data concerning the initial dam-break flow just after the sudden removal of a plate and simulated the flow numerically. Kocaman [76] investigated the effect of lateral channel sidewall contraction on dam-

break flows over horizontal initially dry beds. Cruchaga et al. analyzed fixed mesh finite element approaches to model free surface problems for viscous incompressible Newtonian fluid flows.

Aureli [87] compared the capability of 2D shallow water, 3D Eulerian, and 3D Lagrangian models to predict the impact forces caused by a dam-break wave on a structure. Xu [92] developed an improved smoothed particle hydrodynamics approach and assessed its ability to simulate 3D dam-break flows with breaking waves and Zhang [98] proposed a weakly compressible SPH method based a low-dissipation Riemann solver to model free-surface flow problems with violent wave-breaking and impact events.

3. NUMERICAL METHODS ADOPTED

In the present work, two numerical methods were used:

• **The Material Point Method (MPM):** is an extension of FLIP (Fluid Implicit Particle method) [99], developed by Particle In Cell (PIC) [100]. It is usually used to solve solid mechanics problems with history-dependent variables. MPM can be presented within an Eulerian finite element method (FEM) framework and its equation is reflexed as Lagrangian material points to which information such as the stress and history-dependent variables can be transported. At each time step increment, the position of material points is updated according to the velocities calculated in the Eulerian FEM mesh. In the next time step, the new position will determine the material properties and initial stresses on the corresponding elements [101–103]. The boundary conditions are based on the FEM mesh with fixed nodes (zero velocity) at the domain boundaries. In the present work, no special treatment was adopted for the boundary layer (e.g., wall function), so the wall friction effect is not addressed. The time step is determined based on the background mesh size by the Courant-Friedrichs-Lewy (CFL) condition [104,105].

In Sulsky et al. [106], the governing equations and weak form of the governing equations are presented:

Standard conservation equations for mass and momentum:

$$\frac{\partial \rho}{\partial t} + \rho \nabla \cdot \vec{v} = 0 \,, \tag{1}$$

and

$$\rho \vec{a} = \nabla \cdot \sigma + \rho \vec{b} \,. \tag{2}$$

In equations (1) and (2), $\rho(\vec{x}, t)$ is the mass density; $\vec{a}(\vec{x}, t)$ and $\vec{v}(\vec{x}, t)$ are the acceleration and velocity, respectively; $\sigma(\vec{x}, t)$ is a symmetric stress tensor; and $\vec{b}(\vec{x}, t)$ is the specific body force.

For incompressible flows, the stress tensor [107] is:

$$\sigma_{ij} = -p\delta_{ij} + \mu \, \dot{\varepsilon}_{ij} \,, \tag{3}$$

where μ is the dynamic viscosity of the fluid and the shear rate $\dot{\varepsilon}_{ij}$ is defined by

$$\dot{\varepsilon}_{ij} = \frac{\partial v_i}{\partial x_j} + \frac{\partial v_j}{\partial x_i} \,. \tag{4}$$

Below we describe the discrete formulation of the problem and prescribe the spatial and temporal integration of the equations. In its Lagrangian form, the material is divided into infinitesimal mass elements, where each one has a fixed amount of mass at all times. The coordinates of any point can be written compactly using nodal basis functions as:

$$\vec{x} = \sum_{i=1}^{N_n} \vec{x}_i(t) \, N_i(\vec{x}) \,, \tag{5}$$

where $N_i(x)$ is the element shape function, N_n is the total number of nodes and $\vec{x}_i(t)$ denotes the spatial nodes.

Therefore, the displacement, velocity and acceleration in their nodal form are similar to the equation defined for the coordinates of several points, and the replacement of each variable with the respective functions is performed (see [106]).

The weak form of the motion equation is:

$$\sum_{i=1}^{N_n} \vec{w}_i^k \cdot \sum_{j=1}^{N_n} m_{ij}^k \vec{a}_j^k = -\sum_{j=1}^{N_n} \overline{W}_i^k \cdot$$
$$\sum_{p=1}^{N_p} m_p \sigma_p^{s,k} \cdot \nabla N_i(x)|_{x=X_p^k} + \tag{6}$$
$$\sum_{i=1}^{N_n} \overline{W}_i^k \cdot \hat{t}_i^k + \sum_{i=1}^{N_n} \overline{W}_i^k \cdot \vec{b}_i^k \,,$$

where N_p is the number of material points, k refers to the time step t_k, m_{ij}^k is the matrix mass equation (7) and $\vec{w}_i^k$ are arbitrary components,

except where the components of displacement are prescribed:

$$m_{ij}^k = \sum_{p=1}^{N_p} M_p N_i(\vec{x}_p^k) N_j(\vec{x}_p^k) \,. \tag{7}$$

Included in equation (6), $\vec{b}_i^k$ is the discretized specific body force.

Now we have the weak form of the reduced equation of motion:

$$\sum_{j=1}^{N_n} m_{ij}^k \vec{a}_j^k = \vec{f}_i^{int,k} + \vec{f}_i^{ext,k} \quad, \tag{8}$$

where $\vec{f}_i^{int,k}$ is the internal force vector (9) and $\vec{f}_i^{ext,k}$ is the external force vector (10):

$$\vec{f}_i^{int,k} = -\sum_{p=1}^{N_p} m_p G_{ip}^k \cdot \sigma_p^{s,k} \tag{9}$$

and

$$\vec{f}_i^{ext,k} = \vec{b}_i^k + \hat{t}_i^k \,, \tag{10}$$

where σ^s is the specific stress, $\hat{t}_i^k$ is the discrete applied traction and G_{ip}^k is the gradient of the shape function.

Usually, there are more material points than grid points, in which case a minimum square approach is applied to the mass of the material point to determine the nodal velocities from the velocities at the material points to initialize each time step. The equation in function of the nodal velocities is:

$$\sum_{j=1}^{N_n} m_{ij}^k \vec{v}_j^k = \sum_{p=1}^{N_n} m_p \vec{v}_p^k \, N_i(\vec{x}_p^k) \,, \tag{11}$$

where m_p is the material point mass, $\vec{v}_p^k$ is the velocity of the material point, $\vec{x}_p^k$ is the position of the material point and N_i is the element shape function.

With the equation of motion (8) solved during the Lagrangian phase of the computation, it is necessary to update the solution at the material points of the particle properties, whereby the velocities and positions are updated according to:

$$\vec{v}_p^{k+1} = \vec{v}_p^k + \sum_{i=1}^{N_n} \left[\vec{v}_i^{k+1} - \vec{v}_i^k \right] N_i(\vec{x}_p^k) \tag{12}$$

and

$$\vec{x}_p^{k+1} = \vec{x}_p^k + \Delta t \sum_{i=1}^{N_n} \vec{v}_i^{k+1} N_i(\vec{x}_p^k). \tag{13}$$

It is also necessary to update the deformation gradient for each particle and the stress σ_p.

Finally, to start a new cycle, the information transported by the points of material in a new grid is used, starting a new time step.

• **Smoothed Particle Hydrodynamics (SPH):** is a Lagrangian method based on particles and thus free of mesh [101]. Lucy and Monaghan [108,109] introduced this method to solve astrophysical problems in space with three dimensions. It possesses individual material properties and moves according to the ruling conservation equation [110]. SPH has been studied extensively in the area of fluid dynamics with long deformation, proving very effective and providing high precision. Its main advantage is the natural adaptation achieved at a very early stage based on each time step of the movement history of the arbitrarily distributed particles [101]. Because SPH does not use a mesh, boundary conditions can only be applied by predefined movement of particles located at the domain contours, which is one of the main disadvantages of this method. Therefore, it is based on particles that do not move according to the forces exerted on them, because they remain fixed in their position or move through an already established movement function or objects in motion. When a fluid particle approaches an edge particle (boundary) and the distance between them becomes smaller than twice the length of smoothing, it causes the density of the affected boundary particle to increase, resulting in an increase in pressure. This causes a reverse effect of repulsion exerted on the fluid particle because of the pressure in the moment equation [111]. A variable time step Δt is calculated according to [112], controlled by a Courant and a viscosity condition, where the critical time step is determined by the smallest smoothing length.

Following Monaghan [109], we use the integral representation of the function $A(\vec{r})$:

$$A(\vec{r}) = \int_V A(\vec{r}') \, \delta(\vec{r} - \vec{r}') \, d\vec{r}' \quad , \tag{14}$$

where $A(\vec{r})$ is a continuous function, V is the volume of the integral, $\vec{r}$ is the radius vector, and $\delta(\vec{r} - \vec{r}')$ is the Dirac delta function, defined as:

$$\delta(\vec{r} - \vec{r}') = \begin{cases} 1, & \vec{r} = \vec{r}' \\ 0, & \vec{r} \neq \vec{r}' \end{cases} . \tag{15}$$

The delta function in equation (14) is replaced by the function $W(\vec{r} - \vec{r}', h)$, which is called the smoothing kernel:

$$A_l(\vec{r}) = \int_V A(\vec{r}') \, W(\vec{r} - \vec{r}', h) \, d\vec{r}' \quad , \tag{16}$$

where h is a smoothing radius and W is an interpolating kernel which has two properties, the first being the normalization condition (17) and the second the delta function (18):

$$\int_V W(\vec{r} - \vec{r}', h) \, d\vec{r}' = 1 \tag{17}$$

and

$$\lim_{h \to 0} W(\vec{r} - \vec{r}', h) = \delta(\vec{r} - \vec{r}') . \tag{18}$$

For a discrete number of computational nodes, equation (16) can be replaced by a summation, giving the following expression:

$$A_l(\vec{r}) = \sum_b A_b \, W(\vec{r} - \vec{r}_b, h) \, \Delta V_b \quad , \tag{19}$$

where $\Delta V_b = m_b / \rho_b$ is the volume related to the b th computational node (particle) and $A(\vec{r}')$ is replaced by a set of numbers A_b.

SPH approximation of the arbitrarily continuous function can be derived as:

$$A_s(\vec{r}) = \sum_b m_b \frac{A_b}{\rho_b} W(\vec{r} - \vec{r}_b, h) \quad , \tag{20}$$

where $A_s(\vec{r})$ is the approximated value of function A at the point defined by the radius vector $\vec{r}$.

An approximation of the function gradient $\nabla A(\vec{r})$ is obtained by using the gradient of the smoothing kernel. The approximation is as follows:

$$\nabla A(\vec{r}) = \sum_b m_b \frac{A_b}{\rho_b} \nabla W(\vec{r} - \vec{r}_b, h) \quad , \tag{21}$$

where $\nabla W(\vec{r} - \vec{r}_b, h)$ is the gradient of the kernel function.

Finally, by substituting the SPH approximations for a function and its derivate in the Navier-Stokes equations, the SPH equations of motion can be written as:

$$\frac{d\vec{V}_a}{dt} = -\sum_b m_b \left(\frac{P_b}{\rho_b^2} + \frac{P_a}{\rho_a^2} \right) \nabla_a W_{ab} \tag{22}$$

and

$$\frac{d\rho_a}{dt} = \sum_b m_b \vec{V}_{ab} \nabla_a W_{ab} \tag{23}$$

The purpose of the present work is to contribute to the evaluation of new reliable tools for the prediction of dam-break flows, by comparing the mentioned numerical methods. The simulations reproduced the experimental study of Cruchaga [84] with quadratic and trapezoidal obstacles and also without either of them [58].

The remainder of the article is organized as follows: description of the experimental studies in section 2, simulations of the dam-break models in section 3, comparative analyses of numerical and experimental methods in section 4, and finally some inferences and conclusions based on the results in section 5.

4. DESCRIPTION OF THE CASES STUDIED

In this section, the experimental apparatus from previous studies used here for comparision with the MPM and SPH numerical results is detailed.

First, the Cruchaga [58] experiment of a dam-break flow without obstacles and fixed bed was considered. The experimental design (Fig. 2) consisted of a glass box with a gate, removed at time t = 0 s.
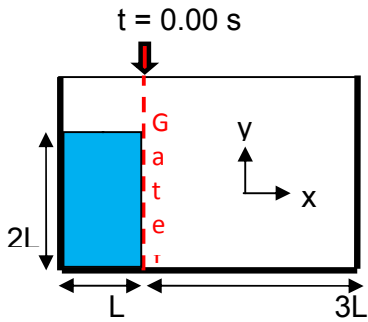
Fig. 2. Model of the experiment, adapted from Cruchaga [58]

The first compartment, with length L = 0.144 m, was filled with water until a height H = 2L. The total length of the box was 4 L.

Furthermore, a few years later Chuchaga [84] performed new experiments in a box with the same dimensions as the previous one and a fixed bed, now including square and trapezoidal obstacles in the water flow path.

The obstacles were located at a distance of 3L/2 after the gate, as represented in Fig. 3,

respectively. In this case, the gate starts to open at a speed v=3.5 m/s.

5. SIMULATIONS OF THE DAM-BREAK MODELS

Two open source computational tools executed the numerical simulations: the NairnMPM [113] and DualSPHysics [114,111] codes, based on the MPM and SPH numerical methods, respectively. Table 1 shows the characteristics of the computer equipment.

Table 1. Computer features

OS	Windows 8.1
Processor	Intel Core, i3-3110M @ 2.40GHz
RAM	4.00 GB
Type of system	64 bits
Video Graphics Card	NVIDIA GeForce GT 620M

Table 2 presents the physical properties of the fluid and Tables 3 (MPM) and 4 (SPH) present the input data of both programs that were used to simulate the dam-break scenarios of this work.
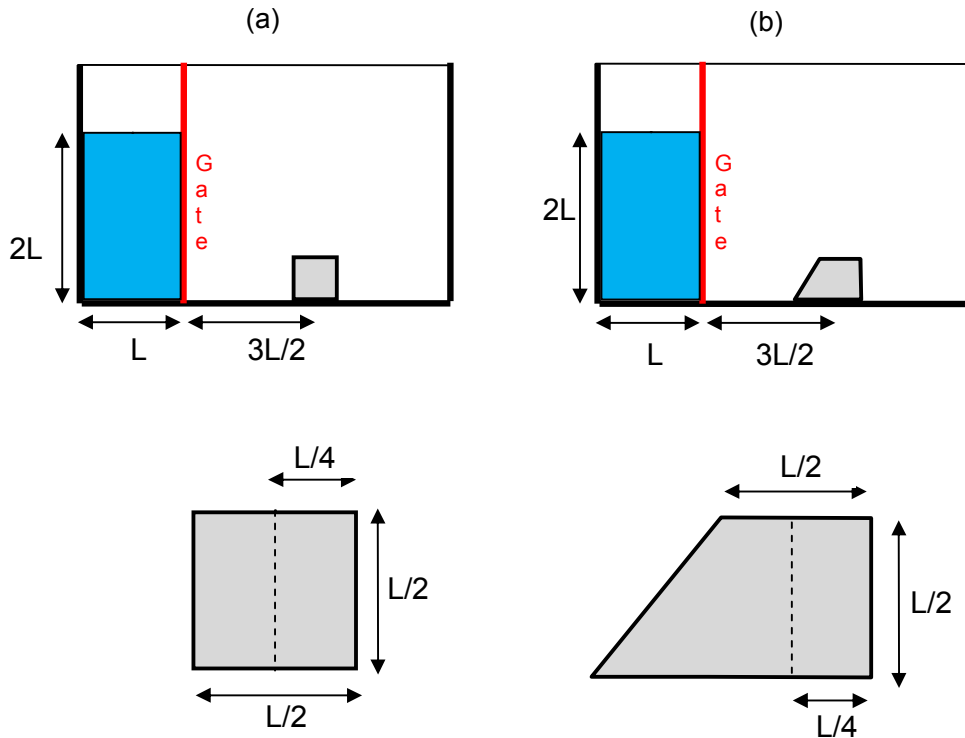
Fig. 3. Position and cross-section of the square (a) and trapezoidal (b) obstacles, adapted from Cruchaga [84]

Table 2. Physical properties

Fluid	Water
Dynamic viscosity	0.001 kg/m/s
Density	1000 kg/m³

Table 3. MPM input data

Courant-Friedrichs-Levy (CFL) number	0.2
Gravity	9.81 m/s²
Time between recorded results	50 ms
Number of steps recorded	24
Volumetric module	21.5 MPa

Table 4. SPH input data

Courant-Friedrichs-Levy (CFL) number	0.2
Gravity	9.81 m/s²
Precision of particle interaction	Double
Coefficient to calculate the smoothing length	1.0
Interaction kernel	Wendland

In order to analyze the results of the MPM and SPH models, six cases were simulated until time t = 1.20 s and the results were compared with the experimental results obtained by Cruchaga [58,84].

Mesh size and model parameters (Tables 2 and 3) were calibrated for each case separately, with the purpose of reproducing in the same way the experiments of Cruchaga. Sensitivity analysis was then performed to assess the influence of mesh size on the numerical predictions, which in the application of this analysis are transformed into very useful information, especially when there are real field applications and the calibration data are not available.

For the experimental model without obstacles [58] and with obstacles [84], the influence of both grid sizes on the numerical results was investigated. For numerical modeling of SPH, by default the software was already defined with a grid size equal to 2 mm, which allowed the flow of the fluid to be similar to the Cruchaga experiments, leaving this value of 2 mm fixed for both experiments, with and without obstacles. Unlike the SPH numerical model, the value of the grid size of the numerical model MPM was not defined by default, so the appropriate value had to be investigated to enter the data in the programming of the software and thus obtain simulations similar to the experimental ones.

For the dam-break flow model in MPM, numerical simulations without obstacles with a coarser ($\Delta x = \Delta y = 10\ mm$) and finer ($\Delta x = \Delta y = 5\ mm$) mesh were carried out along with numerical simulations with obstacles, also having a coarser ($\Delta x = \Delta y = 10\ mm$) and finer ($\Delta x = \Delta y = 2\ mm$) mesh. Below is a brief description of the sensitivity analysis for each case:

Fig. 4 shows the results of the comparisons of the three scenarios: Case 1 - without obstacle [58]; Case 2 - with square obstacle [84]; and Case 3 - with trapezoidal obstacle [84]. The numerical simulations were performed using cell size α = 10 mm for the MPM method (Fig. 4b) and particle size β = 2 mm for the SPH method (Fig. 4c).

In the first three cases, the MPM simulations with cell size α = 10 mm (Fig. 4b) presented divergences with the experimental results. In Case 1, the MPM calculated smaller velocities and a round shape of the front wave, as observed at t = 0.20 s, while the SPH results are visually similar to the experiment for almost all time steps. The same observations apply to cases 2 and 3, with even slower MPM velocities, indicating that this study requires a refined grid (smaller cell size).

In order to improve the MPM results, new simulation studies were carried out.

Without obstacle and cell size set to α = 5 mm (Fig. 5b – Case 4), the MPM presented results significantly better than the previous ones and apparently the same precision as the SPH. However, for the cases with square and trapezoidal obstacles, the MPM required an even more refined grid, with cell size α = 2 mm (Fig 5b* – Cases 5 and 6).

The water flow at time step t = 0.40 s (Fig. 5) reached nearly the same maximum height for all analyzed methods, which indicates that the point/particle velocities calculated are also consistent.

Compared to the square obstacle case, the trapezoidal geometry provided a ramp to the flow that decreased the maximum height (t = 0.4 s), while on the other hand it increased the horizontal velocity, as shown by the amount of water that overpassed the obstacle until t = 0.6 s. Once again, these observations are compatible with the results from both numerical methods, MPM and SPH.

(a) Exp. (b) MPM (c) SPH　　**(a) Exp. (b) MPM (c) SPH**　　**(a) Exp. (b) MPM (c) SPH**
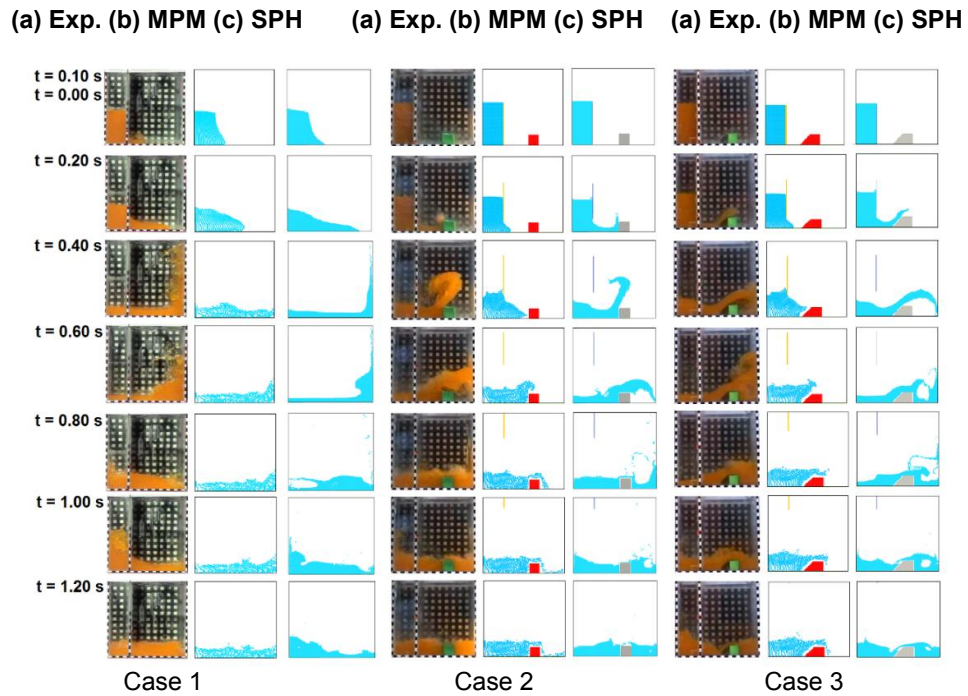
Fig. 4. Comparison between experimental data of Cruchaga [58,84] (a), MPM with α = 10 mm (b) and SPH with β = 2 mm (c) in the three scenarios: Case 1 – without obstacle; Case 2 – with square obstacle; Case 3 – with trapezoidal obstacle

(a) Exp. (b) MPM (c) SPH　　**(a) Exp. (b*) MPM (c) SPH**　　**(a) Exp. (b*) MPM (c) SPH**
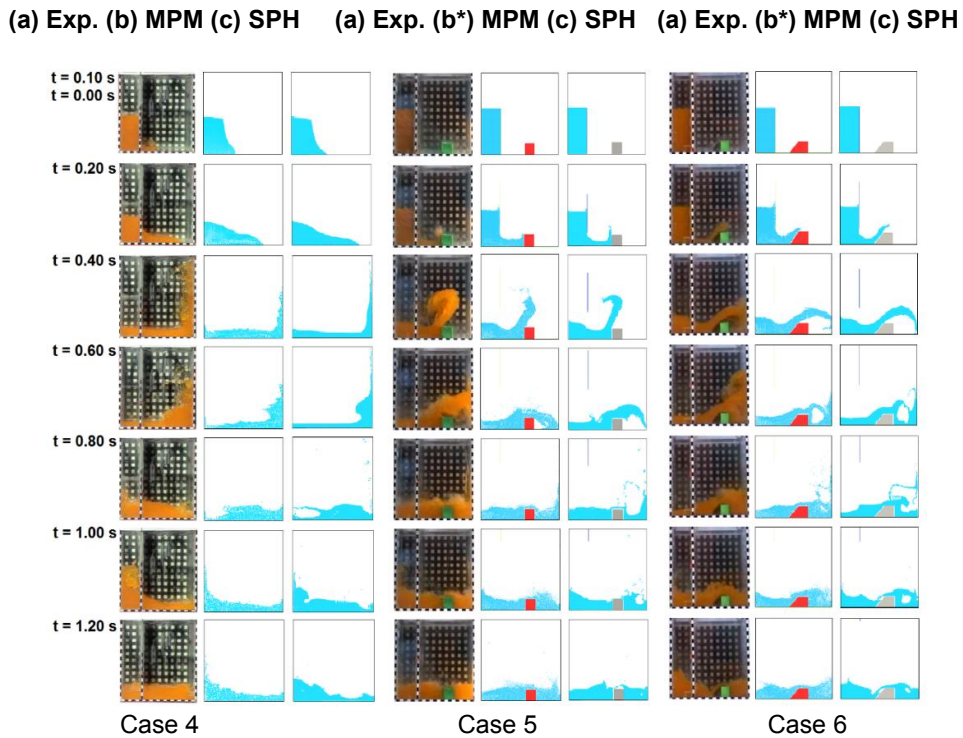
Fig. 5. Results of Cruchaga dam-break experiment [58,84], MPM with α = 5 mm (b), α = 2 mm (b*) and SPH with β = 2 mm (c)

6. PERFORMANCE OF THE NUMERICAL METHODS USED HERE

In order to make a more comprehensive comparison between the applied methods, this section analyzes the computational cost of each one. The first comparative analysis considered only cases 4, 5 and 6, whose simulations are closer to the experimental results. Table 5 presents the computational cost of the MPM and SPH methods.

The computational cost of MPM is between two and three orders of magnitude greater than SPH. This is due to the way each method works. The MPM executes the whole calculation area of the simulation through the finite element method (FEM), where all the information is loaded by the material points of the mesh, thus requiring a higher computational cost. Therefore, the greater the number of points that the MPM simulation concentrates (case 5 and case 6), the longer the simulation time will be.

On the other hand, SPH is dedicated to computational fluid dynamics (CFD) and free mesh, with the disadvantage of not working with edge conditions, but when performing the referred case study based on a fluid, the simulation computational cost is lower than that of the MPM (Fig. 6).

Table 5. Computational cost

MPM - EXECUTION TIMES			
	No Obstacle (Case 4)	Square Obstacle (Case 5)	Trapezoidal Obstacle (Case 6)
Simulation steps	173665	437966	437966
Simulation runtime (s)	5273	146405	151350
Simulation runtime (min)	87.88	2440.09	2522.50
Step per millisecond (ms)	30	334	346
Number of material points	4774	31174	32770
Calculation time step (μs)	6.910	2.740	2.740
Archiving time step (s)	0.2	0.2	0.2
SPH - EXECUTION TIMES			
	No Obstacle (Case 4)	Square Obstacle (Case 5)	Trapezoidal Obstacle (Case 6)
Simulation steps	71581	70248	67552
Simulation runtime (s)	349	457	360
Simulation runtime (min)	5.82	7.62	6.00
Steps per second (s)	205	154	188
Number of particles	7183	8053	8455
Calculation time step (μs)	16.76	17.08	17.76
Archiving time step (s)	0.2	0.2	0.2
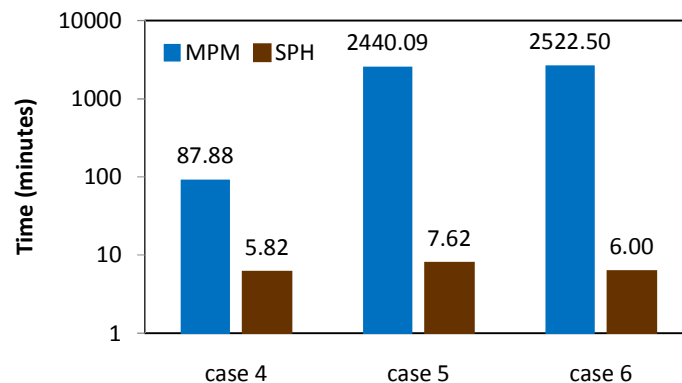
Fig. 6. Execution time in minutes of MPM (blue) and SPH (orange)

The average execution times for the three cases were 6.5 minutes for the SPH model and 1683.5 minutes for the MPM. The difference in the MPM execution time of case 4, compared to cases 5 and 6, is due to the reduced cell size, which was necessary for the last two cases to preserve acceptable result quality of the models with obstacles (square and trapezoidal).

It is important to mention that the different cell sizes (α) for the MPM (cases 1, 2 and 3 with α = 10 mm; case 4 with α = 5 mm and cases 5 and 6 with α = 2 mm) were chosen intentionally to keep the computational cost as low as possible for each case. Therefore, that parameter was adjusted until it reached the required level. In the SPH, β = 2 mm was used for all cases, since a smaller particle size did not produced significantly better results.

7. CONCLUSIONS

Based on the simulations of dam-break flow calculated with the MPM and SPH methods, compared to the experimental data, [58] and [84], the following conclusions are highlighted:

- For the SPH simulations, the particle size β $\leq$ 2 mm provided results with acceptable accuracy, corresponding to a ratio between β and the total length of the model equal to 2/576.
- To obtain acceptable results from the MPM with obstacles, a grid cell size α ≤ 2 mm was necessary, which corresponds to a ratio between α and the total length of the model equal to 1/288 (288 cells per horizontal line).
- For all cases analyzed, the SPH presented greater computational efficiency, requiring calculation time two to three orders of magnitude smaller than the MPM. Therefore, it is the most suitable method for the referred type of simulation.
- However, the MPM is based on FEM, so it can model many different types of materials, allowing simulations that account for the interaction between fluids and complex structures. On the other hand, the SPH method was developed specifically for fluids or materials that behave like fluids (e.g., submarine landslides), thus restricting its applicability.
- Finally, both numerical methods used in this work (MPM and SPH) provided results very close to the experimental studies of Cruchaga [58,84]. Therefore, those methods are potential tools for the prediction of dam-break flows and, consequently also for the prevention and mitigation of this type of disaster.

COMPETING INTERESTS

Authors have declared that no competing interests exist.

REFERENCES

1. Hyndman D. Natural Hazards And Disasters, Second Edition; 2009.
2. Davies R. UN – 1995 to 2015, Flood Disasters Affected 2.3 Billion and Killed 157,000 – FloodList", Flood Recovery; 2015.
   Available:http://floodlist.com/dealing-with-floods/flood-disaster-figures-1995-2015 [Acessado: 29-set-2017].
3. Saxena KR, Dams: Incidents and accidents. A.A. Balkema; 2005.
4. M Zagonjolli. Dam break modelling, risk assessment and uncertainty analysis for flood mitigation; 2007.
5. Y Si. The World's Most Catastrophic Dam Failures; 1998.
6. Singh VP, Quiroga C. A dam-breach erosion model: I. Formulation, Water Resour. Manag. 1987;1(3):177–197,.
7. Singh VP, Quiroga CA. Dimensionless analytical solutions for dam-breach erosion. J. Hydraul. Res. J. J. Hydraul. Res. 1988;26(2):22–1686.
8. Foda MA, Hill DF, DeNeale PL, Huang CM. Fluidization response of sediment bed to rapidly falling water surface", Waterw. Port, coastal, Ocean Eng.; 1997.
9. Jaeggi MN, Pellandini S. Torrent check dams as a control measure for debris flows, in Recent Developments on Debris Flows, Berlin, Heidelberg: Springer Berlin Heidelberg. 1997;186–207.
10. Capart H, Young DL. Formation of a jump by the dam-break wave over a granular bed. J. Fluid Mech. 1998;372. S0022112098002250, out.

11. Bellos C, Hrissanthou V. Numerical simulation of sediment transport following a Dam Break. Water Resour. Manag; 1998.
12. David P, Andrew H. On sediment transport under dam-break flow. J. Fluid Mech. 2002;473:265–274,.
13. Fraccarollo L, Capart H. Riemann wave description of erosional dam-break flows, J. Fluid Mech. 2002;461:183–228.
14. Leal J, R Ferreira, A Cardoso. DamBreak waves on movable bed; 2002.
15. Ling L, Ni J, Borthwick A. Simulation of dike-break processes in the Yellow River. Sci. China; 2002.
16. Joao L, Rui F, AntonioC. Dam-Break wave propagation over a cohesionless erodible bed; 2003.
17. Zhixian C, Gareth P, Steve W, Paul C, Computational DamBreak hydraulics over erodible sediment bed. Hydraul. Eng; 2004.
18. Faeh R. Numerical modeling of breach erosion of river embankments. J. Hydraul. Eng. 2007;133(9):1000–1009.
19. Zech Y, S Soares-Frazão, B Spinewine, Le Grelle N. Dam-break induced sediment movement: Experimental approaches and numerical modelling. J. Hydraul. Res. 2008;46(2):176–190.
20. Wu W, Wang SSY. One-dimensional explicit finite-volume model for sediment transport", J. Hydraul. Res. 2008;46(1):87–98.
21. Bohorquez P, Fernandez-Feria R. Transport of suspended sediment under the dam-break flow on an inclined plane bed of arbitrary slope. 2008;22:2615–2633.
22. El Kadi Abderrezzak K, Paquier A. Applicability of sediment transport capacity formulas to dam-break flows over movable beds. J. Hydraul. Eng. 2011;37(2):209–221.
23. Zhang M, Wu WM. A two dimensional hydrodynamic and sediment transport model for dam break based on finite volume method with quadtree grid. Appl. Ocean Res. 2011;33(4):297–308.
24. Shakibaeinia A, Jin YC. A mesh-free particle model for simulation of mobile-bed dam break. Adv. Water Resour. 2011; 34(6):794–807.
25. Goutiere L, Soares-Frazão S, Y Zech. Dam-break flow on mobile bed in abruptly widening channel: Experimental data. J. Hydraul. Res. 2011;49(3):367–371.
26. Lin P, Wu Y, Bai J, Lin Q. A numerical study of dam-break flow and sediment transport from a quake lake. J. Earthq. Tsunami. 2011;5(5):401–428.
27. Li J, Cao Z, Pender G, Liu Q. A double layer-averaged model for dam-break flows over mobile bed. J. Hydraul. Res. 2013;51(5):518–534.
28. Evangelista S, Altinakar MS, Di Cristo C, Leopardi A. Simulation of dam-break waves on movable beds using a multi-stage centered scheme. Int. J. Sediment Res. 2013;28(3):269–284.
29. Huang W, Cao Z, Paul C, Gareth P. Coupled 2D hydrodynamic and sediment transport modeling of megaflood due to glacier Dam-Break in Altai Mountains, Southern Siberia; 2014.
30. Qihua R, Jian T, Songdong S, Xudong F, Yueping X, Incompressible SPH scour model for movable bed Break Flows; 2015.
31. DH Kim. H2D morphodynamic model considering wave, current and sediment interaction, Coast. Eng. 2015;95:20–34.
32. Huang W, Cao Z, Pender G, Liu Q, Carling P. Coupled flood and sediment transport modelling with adaptive mesh refinement; 2015.
33. Ortiz P, Anguita J, Riveiro M. Free surface flows over partially erodible beds by a continuous finite element method. Environ. Earth Sci. 2015;74(11):7357–7370,
34. Evangelista S. Experiments and numerical simulations of dike erosion due to a wave impact. Water (Switzerland). 2015;7(10): 5831–5848.
35. Fu L, Jin YC. Improved multiphase lagrangian method for simulating sediment transport in dam-break flows. J. Hydraul. Eng. 2016;142(6):4016005.
36. Di Cristo C, Evangelista S, Greco M, Iervolino M, Leopardi A, Vacca A. Dam-break waves over an erodible embankment: Experiments and simulations. J. Hydraul. Res. 2017;1686:1–15.
37. Martin JC, Moyce WJ. Part IV. An experimental study of the collapse of liquid columns on a rigid horizontal plane. Source Philos. Trans. R. Soc. London. Ser. A Math. Phys. Sci. 1952;244(882):312–324.
38. Dressler RF. Hydraulic resistance effect upon the dam-break functions. J. Res. Natl. Bur. Stand. 1934;49(3): 1952.

39. Dressler RF, Comparison of theories and experiments for the hydraulic Dam-break wave; 1954.

40. Xanthopoulos T, Koutitas C. Numerical simulation of a two dimensional flood wave propagation due to dam failure. J Hydraul. Res. 1976;14(4):321–331.

41. Katopodes ND, Schamber DR, Applicability of dam-break flood wave models. J. Hydraul. Eng. 1983;109(5):702–721.

42. Townson JM, Al-Salihi AH. Models of dam-break flow in R-T space. J. Hydraul. Eng. 1989;115(5):561–575. maio

43. Beiios CV, Soulis JV, Sakkas JG. Computation of two-dimensional dam-break- induced flows. Comput. Mech. Publ; 1990.

44. Soulis JV. Computation of two-dimensional dam-break flood flows. Int. J. Numer. Methods Fluids. 1992;14(6):631–664.

45. Fraccarollo L, Toro EF. Experimental and numerical assessment of the shallow water model for two-dimensional dam-break type problems. J. Hydraul. Res. 1995;33(6): 843–864.

46. Koshizuka S, Oka Y. Moving-particle semi-implicit method for fragmentation of incompressible fluid; 1996.

47. Stansby P, Chegini A, Barnes T. The initial stages of dam-break flow. Fluid Mech; 1998.

48. Wang Z, Shen HT. Lagrangian simulation of one-dimensional dam-break flow. J. Hydraul. Eng. 1999;125(11):1217–1220.

49. Colicchio G, Colagrossi A, Greco M, Landrini M. Free-surface flow after a dam-break: A comparative study; 2002.

50. Petaccia G, Savi F. Two dimensional simulation of a dam break wave propagation for the isolated building test case; 2003.

51. Soares S, Noel B. Experiments of dam-break flow in the precense of obstacles; 2004.

52. Walhorn E, Kölke A, Hübner B, Dinkler D. Fluid–structure coupling within a monolithic model involving free surface flows. Comput. Struct. 2005;83:25–26:2100–2111.

53. Quecedo M, Pastor M, Herreros MI, Merodo JAF, Zhang Q. Comparison of two mathematical models for solving the dam break problem using the FEM method. Comput. Methods Appl. Mech. Eng. 2005; 194(36–38):3984–4005.

54. Kleefsman KMT, Fekken G, Veldman AEP, Iwanowski B, Buchner B. A volume-of-fluid based simulation method for wave impact problems. J. Comput. Phys. 2005;206: 363–393,

55. Greaves DM. Simulation of viscous water column collapse using adapting hierarchical grids. Int. J. Numer. Methods Fluids. 2006;50(6):693–711.

56. Soares-Frazão S. Experiments of dam-break wave over a triangular bottom sill. J. Hydraul. Res. 2007;45(sup1):19–26dez.

57. Soares-Frazão S, Zech Y. Experimental study of dam-break flow against an isolated obstacle. J. Hydraul. Res. 2007; 45(sup1):27–36.

58. Cruchaga MA, Celentano DJ, Tezduyar TE. Collapse of a liquid column: Numerical simulation and experimental validation. Comput. Mech. 2007;39:453–476.

59. Larese A, Rossi R, Oñate E, Idelsohn S. Validation of the particle finite element method (PFEM) for simulation of free surface flows; 2008.

60. Soares-Frazão S, Zech Y. Dam-break flow through an idealised city. J. Hydraul. Res. 2008;46(5):648–658.

61. Zhang Y, Zou Q, Greaves D. Numerical simulation of free-surface flow using the level-set method with global mass correction. Int. J. Numer. Methods Fluids. p. n/a-n/a; 2009.

62. Zhou JT, Ma QW, Zhang L, Yan S. Numerical investigation of violent wave impact on offshore wind energy structures using MLPG_R method; 2009.

63. WU TR, LIU PLF. Numerical study on the three-dimensional dambreak bore interacting with a square cylinder. In Nonlinear Wave Dynamics, World Scientific. 2009;281–303.

64. Park IR, Kim KS, Kim J, Van SH. A volume-of-fluid method for incompressible free surface flows. Int. J. Numer. Methods Fluids. 2009;61(12):1331–1362,dez.

65. Lee ES, Violeau D, Issa R, Ploix S. Application of weakly compressible and truly incompressible SPH to 3-D water collapse in waterworks. J. Hydraul. Res. 2010;48(sup1):50–60.

66. Ryzhakov PB, Rossi R, Idelsohn SR, Oñate E. A monolithic Lagrangian approach for fluid–structure interaction problems. Comput Mech. 2010;46:883–899.

67. Kassiotis C, Ibrahimbegovic A, Matthies H. Partitioned solution to fluid-structure

interaction problems in applicaion to free-surface flows; 2010.

68. Xia J, Falconer RA, Lin B, Tan G. Modelling flood routing on initially dry beds with the refined treatment of wetting and drying. Int. J. River Basin Manag. 2010;8(3–4):225–243,dez.

69. Ferrari A, Fraccarollo L, Dumbser M, Toro EF, Armanini A. Three-dimensional flow evolution after a dam break. J. Fluid Mech. 2010;663:456–477.

70. Ozmen-Cagatay H, Kocaman S. Dam-break flows during initial stage using SWE and RANS approaches. J. Hydraul. Res. 2010;48(5):603–611,out.

71. Yang C, Lin B, Jiang C, Liu Y. Predicting near-field dam-break flow and impact force using a 3D model. J. Hydraul. Res. 2010; 48(6):784–792,dez.

72. Biscarini C, Di Francesco S, Manciola P. CFD modelling approach for dam break flow studies. Hydrol. Earth Syst. Sci. 2010; 14:705–718,

73. Singh JMS, Altinakar, Ding Y. Two-dimensional numerical modeling of dam-break flows over natural terrain using a central explicit scheme. Adv. Water Resour. 2011;34(10):1366–1375,out.

74. Singh J, Altinakar MS, Ding Y. Two-dimensional numerical modeling of dam-break flows over natural terrain using a central explicit scheme. Adv. Water Resour. 2011;34(10):1366–1375.

75. Ozmen-Cagatay H, Kocaman S. Dam-break flow in the presence of obstacle: Experiment and CFD simulation. Eng. Appl. Comput. Fluid Mech. 2011;5(4):541–552.

76. Kocaman S, Ozmen-Cagatay H. The effect of lateral channel contraction on dam break flows: Laboratory experiment. J. Hydrol. 2012;432–433:145–153, abr.

77. Koh CG, Gao M, Luo C. A new particle method for simulation of incompressible free surface flow problems. Int. J. Numer. Methods Eng. 2012;89(12):1582–1604.

78. Oertel M, Bung DB. Initial stage of two-dimensional dam-break waves: Laboratory versus VOF. J. Hydraul. Res. 2012;50(1): 89–97.

79. Lobovsk L, Botia-Vera E, Castellana F, Mas-Soler J, Souto-Iglesias A. Experimental investigation of dynamic pressure loads during dam break; 2013.

80. Liu X, Xu H, Shao S, Lin P. An improved incompressible SPH model for simulation of wave–structure interaction. Comput. Fluids. 2013;71:113–123.

81. Wu J, Dalrymple RA. Simulating dam-break flooding with floating objects through intricate city layouts using GPU-based SPH method. 2013;III.

82. Hänsch S, Lucas D, Höhne T, Krepper E. Application of a new concept for multi-scale interfacial structures to the dam-break case with an obstacle. Nucl. Eng. Des. 2014;279:171–181.

83. Casulli V. A semi-implicit numerical method for the free-surface Navier-Stokes equations. Int. J. Numer. Methods Fluids. 2014;74(8):605–622.

84. Cruchaga M, Battaglia L, Storti M, JD 'elía. Numerical modeling and experimental validation of free surface flow problems; 2014.

85. Marsooli R, Wu W. 3-D finite-volume model of dam-break flow over uneven beds based on VOF method. Adv. Water Resour., 2014;70(August):104–117.

86. Ozmen-Cagatay H, Kocaman S, Guzel H. Investigation of dam-break flood waves in a dry channel with a hump. J. Hydro-Environment Res. 2014;8(3):304–315.

87. Aureli F, Dazzi S, Maranzoni A, Mignosa P, Vacondio R. Experimental and numerical evaluation of the force due to the impact of a dam-break wave on a structure. Adv. Water Resour. 2015;76: 29–42.

88. Mao S, Chen Q, Li D, Feng Z. Modeling of free surface flows using improved material point method and dynamic adaptive mesh refinement. J. Eng. Mech. 2015;July: 4015069.

89. Kumar P, Yang Q, Jones V, Mccue-Weil L. ScienceDirect IUTAM Symposium on particle methods in fluid mechanics coupled SPH-FVM simulation within the OpenFOAM framework. Procedia IUTAM. 2015;18:76–84.

90. Kocaman S, Ozmen-Cagatay H. Investigation of dam-break induced shock waves impact on a vertical wall. J. Hydrol. 2015;525(March):1–12.

91. Tang Z, Wan D, Chen G, Xiao Q. Numerical simulation of 3D violent free-surface flows by multi-resolution MPS method. J. Ocean Eng. Mar. Energy. 2016; 2(3):355–364,ago.

92. Xu X. An improved SPH approach for simulating 3D dam-break flows with breaking waves. Comput. Methods Appl. Mech. Eng. 2016;311:723–742.

93. Albano R, Sole A, Mirauda D, Adamowski J. Modelling large floating bodies in urban area flash-floods via a Smoothed Particle Hydrodynamics model. J. Hydrol. 2016; 541:344–358.

94. Jian W, Liang D, Shao S, Chen R, Yang K. SPH simulations of dam-break flows around movable structures; 2016.

95. Kularathna S, Soga K. Implicit formulation of material point method for analysis of incompressible materials. Comput. Methods Appl. Mech. Eng. 2017;313:673–686, jan.

96. Zhao X, Liang D, Martinelli M. ScienceDirect numerical simulations of dam-break floods with MPM. Procedia Eng. 2017;175:133–140.

97. Gu S, et al. SWE-SPHysics simulation of dam break flows at south-gate gorges reservoir. Water. 2017;9(6):387.

98. Zhang C, Hu XY, Adams NA. A weakly compressible SPH method based on a low-dissipation Riemann solver. J. Comput. Phys. 2017;335(May):605–620.

99. Brackbill JU, Kothe DB, Ruppel HM. Flip: A low-dissipation, particle-in-cell method for fluid flow. Comput. Phys. Commun. 1988; 48(25).

100. Sulsky Z. Chen, Schreyer HL. A particle method for history-dependent materials; 1993.

101. Liu GR, Liu MB. Smoothed particle hydrodynamics. World Scientific; 2003.

102. Deborah S, Howard L. Axisymmetric form of the material point method with applications to upsetting and Taylor impact problems. Comput. Methods Appl. Mech. Eng. 1996;139(1–4):409–429,dez.

103. Luis Muller A,Lucas Ludeña Gutierrez. Formulação e algumas aplicações do MPM (Material Point Method) em problemas de geotecnia em condições estáticas e dinâmicas; 2016.

104. Sulsky D, Kaul A. Implicit dynamics in the material-point method; 2003.

105. Ma S, Zhang X, Qiu XM. Comparison study of MPM and SPH in modeling hypervelocity impact problems. Int. J. Impact Eng. 2009;36(2):272–282.

106. Sulsky D, Zhou SJ, Schreyer HL. Application of a particle-in-cell method to solid mechanics. Comput. Phys. Commun. 1995;87(1–2):236–252,maio.

107. Landau L, Lifshitz E. Fluid mechanics 2nd Edition Pergamon Press; 1987.

108. LB L. A numerical approach to the testing of the fission hypothesis. The Astronomical Journal; 1977.
Available:https://scholar.google.com.br/scholar?hl=pt-BR&as_sdt=0%2C5&q=Lucy%2C+L%2C+B.+1977.+Astron.+J.+82%3B+1013&btnG=
[Acessado: 24-out-2017].

109. Monaghan JJ. Smoothed particle hydrodynamics. Annu. Rev. Astron. Astrophys. 1992;30(1):543–574,set.

110. Liu MB, Liu GR. Smoothed particle hydrodynamics (SPH): An overview and recent developments. Arch Comput Methods Eng. 2010;17:25–76.

111. Crespo A, et al. DualSPHysics: Open-source parallel CFD solver based on Smoothed Particle Hydrodynamics (SPH). Comput. Phys. Commun. 2015;187(187): 204–216.

112. Monaghan JJ, Kos A. Solitary waves on a cretan beach. Waterw. port, coastal, Ocean Eng.; 1999.

113. Nairn JA. NairnFEAMPM - OSUPDOCS; 2017.

114. DualSPHysics: GPU and OpenMP based SPH; 2018.